Highly Efficient 3D Nonlinear Photonic Crystals in Ferroelectrics

Shan Liu, Lei Wang, Leszek Mazur, Krzysztof Switkowski, Bingxia Wang, Feng Chen,* Ady Arie, Wieslaw Krolikowski, and Yan Sheng*

Nonlinear photonic crystals (NPCs) with spatially modulated second-order nonlinear coefficients are indispensable in nonlinear optics and modern photonics. To access full degrees of freedom in the generation and control of coherent light at new frequencies, three dimensional (3D) NPCs have been recently fabricated employing the femtosecond laser writing technique in ferroelectric crystals. However, the nonlinear interaction efficiencies in 3D NPCs so far are rather low, which has been a major barrier to further development. Here, fabrication challenges of large-scale 3D NPCs have been overcome to realize more than four orders of magnitude efficiency improvement over previously reported crystals. With the generation of second harmonic vortex beam as an example, the measured conversion efficiencies as high as 2.9×10^{-6} W^{-1} (femtosecond pulse-pumped) and 1.2×10^{-5} W^{-1} (continuous-wave-pumped) are comparable with those in 1D or 2D NPCs. A general approach of structural simplification to relax fabrication challenge of truly complex 3D structures without sacrificing the predesigned functions is also presented. This realization of efficient nonlinear interactions in 3D NPCs paves the way for their novel applications in nonlinear photonics and quantum optics including nonlinear orbital angular momentum multiplexing and high-dimensional entangled source.

1. Introduction

Optical parametric processes, which typically include second harmonic generation (SHG), optical parametric oscillation and amplification, and spontaneous parametric down conversion, are of great importance to the generation and control of both, classical and quantum light sources at new frequencies. It is well known the efficiency of optical parametric processes critically depends on the phase matching condition, which ensures constructive interference of the generated signals throughout the whole sample. This can be achieved by employing the quasi-phase-matching (QPM) technique in nonlinear photonic crystals (NPCs), which utilizes a spatial modulation of the second-order nonlinearity ($\chi^{(2)}$) of the medium to synchronize the phases of the interacting waves. [1–2] 1D and 2D NPCs have been routinely fabricated using the electric field poling of ferroelectric crystals such as LiNbO$_3$ or LiTaO$_3$.[3–8] However, the formation of 3D NPCs had been a challenge for years until the recent usage of near-infrared femtosecond laser pulses to engineer second-order nonlinear coefficient in three dimensions.[9–12]

The increased dimensionality offered by 3D NPCs enables new phase matching schemes such that the nonlinear interactions can be controlled in manners that were not accessible before.[13] For instance, the 3D NPCs have been used to demonstrate volume nonlinear holography, QPM multiplexing and de-multiplexing, dynamic nonlinear wave-front shaping, and

S. Liu, W. Krolikowski, Y. Sheng
Quantum Science and Technology
Research School of Physics
Australian National University
Canberra, ACT 2601, Australia
E-mail: yan.sheng@anu.edu.au

L. Wang, F. Chen
School of Physics
Shandong University
Jinan 250100, China
E-mail: drfchen@sdu.edu.cn

L. Mazur
Faculty of Physics
Warsaw University of Technology
Koszykowa 75, Warsaw 00-662, Poland

K. Switkowski, W. Krolikowski
Division of Arts & Science
Texas A&M University at Qatar
Doha Qatar

B. Wang, Y. Sheng
Laboratory of Infrared Materials and Devices
Research Institute of Advanced Technologies
Ningbo University
Ningbo 315211, China

A. Arie
School of Electrical Engineering
Fleischman Faculty of Engineering
Tel Aviv University
Tel Aviv 69978, Israel

**ADVANCED
SCIENCE NEWS**

www.advancedsciencenews.com

**ADVANCED
OPTICAL
MATERIALS**

www.advopticalmat.de

parallel multi-wavelength frequency conversion.[14–16] They also have great potentials for generations of high dimensional entangled states in the spatial basis and for the exploration of optical analogues of spin dynamics in magnetization textures, such as the topological Hall effect.[17–19]

However, the efficiency of nonlinear optical interactions in 3D NPCs demonstrated so far has been extremely low, which severely limits their potential applications. For example, the reported normalized efficiency of the second harmonic vortex beam generation in the periodic fork-like 3D NPC was 1.4×10^{-10} W^{-1}, and the efficiency of nonlinear beam shaping in 3D multiplexing hologram was 4.25×10^{-11} W^{-1}. [15,20] For comparison, the normalized efficiency of the second harmonic Airy beam in an electric-field poled 2D NPC can be as high as 10^{-5} W^{-1}. [6] Several major challenges remain to achieve more efficient nonlinear interactions in 3D NPCs. For one, the laser writing method needs to be optimized to be able to write deeper into the second-order nonlinear crystals to support the fabrication of large-scale 3D NPCs. Due to the spherical aberrations and the influence of the birefringence of nonlinear optical crystals, the writing laser beam cannot be perfectly focused deep inside a high refractive index crystal. Hence the previously reported 3D NPCs are generally of small size on the scale of 100–200 µm. There is also a need to reduce the undesired modification of the linear refractive index by the laser writing process, as it leads to reflection, linear diffraction and scattering losses of waves that limit the effective interaction length in the NPCs.[13] Furthermore, 3D NPCs usually suffer from more severe structural errors than their low-dimensional counterparts because they are inherently complex. Potential difference between the real and ideal structures will have detrimental effect on the performance of the former, preventing them, in the extreme case, from performing the expected nonlinear optical functions.[16]

In this work, we demonstrate more than four orders of magnitude efficiency improvement of nonlinear interactions in 3D NPC, with the generation of second harmonic vortex beam being taken as an example. A polarization sensitive femtosecond laser writing approach is proposed to form ferroelectric domain structures deep inside the crystal for fabricating large-scale NPCs. Meanwhile, the manufacturing parameters such as the focusing condition and writing powers are optimized to reduce the modification of the linear index by the laser writing process, so the reflections and scattering of interacting waves caused by these modifications can be reduced and the efficiency of nonlinear interaction can be improved by using longer interaction distance. To simplify the writing process and to avoid fabrication errors, rather than pursue the perfect structure, a fabrication friendly structure is designed and fabricated. Moreover, this structure is phase matched for an on-axis process, and the generated second harmonic is obtained at a single direction in the far field.[21] This scheme is therefore inherently more efficient than previous off-axis designs, where the efficiency was reduced owing to non-collinear process and to the splitting of the second harmonic signal into multiple orders in the far field.[20] The Laguerre-Gaussian (LG) mode laser beams are realized at new wavelength, with the measured conversion efficiency exceeding 2.9×10^{-6} W^{-1} from a femtosecond laser pump and 1.2×10^{-5} W^{-1} from a continuous wave (CW) laser pump.
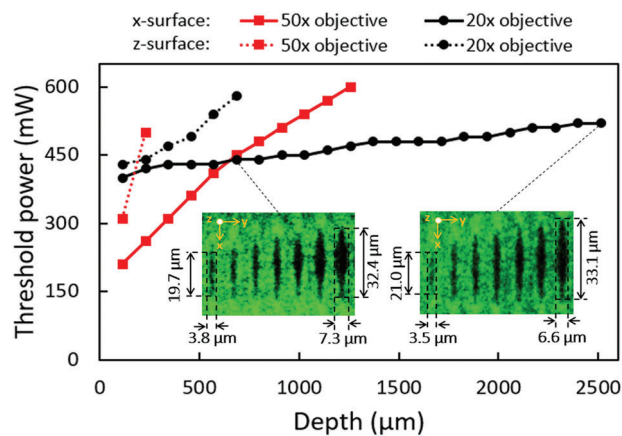

Figure 1. The influences of the polarization of the writing beam with respect to the crystallographic orientation and the focusing condition on the light-induced ferroelectric domain inversion. The threshold power is defined as the minimal laser power that can induce domain inversion at the corresponding depth inside the crystal. Inserted images are the Čerenkov second harmonic microscopic images of the laser written domains at depths of 686 µm (left) and 2628 µm (right), respectively, obtained with the incidence of writing laser from x-surface and focused by a 20× objective lens.

2. Results

2.1. Domain Writing Deep into the Second-Order Nonlinear Optical Crystal

Femtosecond laser writing in second-order nonlinear crystals is challenging because most of these crystals are birefringent and have high refractive index. Due to the birefringence, the focal point of the tightly focused laser beam will split into multiple foci inside the crystal and significantly reduces the laser writing quality, especially when focused deep inside the sample.[22] To overcome this restriction, we used the ordinarily polarized writing laser beam and ensured that the light travels at the same refractive index after tight focusing in the laser writing process. In experiment, we carried out femtosecond laser writing in an as-grown calcium barium niobate ($Ca_{0.28}Ba_{0.72}Nb_2O_6$, CBN) crystal. As elaborated,[22] the single focus condition can be achieved by using the ordinary polarized writing beam incident from the x surface of the crystal. For comparison, the incidence of the ordinary light from z surface was also investigated using the same poling parameters. **Figure 1** shows the dependences of the laser poling thresholds on the writing depth inside the crystal for both cases, respectively. It is clearly seen the incidence of laser beam from x surfaces lead to ferroelectric domain inversion much deeper than those from z-surface which suffered from focus splitting, owing to the crystal birefringence. Focused by a 20× objective lens, the ordinary light incident from x-surface led to domain inversion as deep as 2628 µm below the surface. Along with the writing depths changing from 114 to 2628 µm, the poling threshold power was gradually increased from 400 to 520 mW. We expect that the maximum laser poling depth could even exceed 2628 µm using this poling method, but the working distance of the used 20× objective did not allow us to test it further. On the contrary, the incidence of writing beam from the z
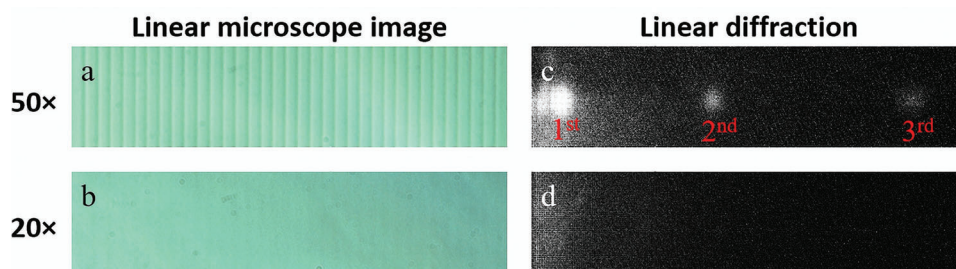
Figure 2. Modifications of the refractive index for different focusing conditions of the poling laser beam. Top and bottom row: poling with 50× and 20× objective lens, respectively. a,b) Optical microscopic images of the nonlinear gratings, respectively. c,d) The corresponding linear optical diffraction patterns. Notice the lack of diffraction from poling with 20× objective.

surface cannot result in any domain structures beyond depth of 600 µm, even though the laser power was increased to the maximum (600 mW). This was caused by the unavoidable focus splitting of the tightly focused beam.[22]

The inserts in Figure 1 depict the nonlinear optical microscope images of the laser poled domain structures obtained at the depths of 686 µm (left) and 2628 µm (right), respectively, with the beam incident from x-facet of the crystal. The dark regions in these images represent the laser induced ferroelectric domains with uniform spontaneous polarizations.[23] There are seven stripe-like domains in each image, with the left one being poled with threshold power and the sequent domains on the right side were poled with power increasing in 10 mW increments. It can be seen the domain structures created at these two depths have very similar qualities and sizes, indicating the possibility to fabricate large-scale NPCs for versatile applications with higher efficiencies.

The influence of different focusing conditions on the threshold power of ferroelectric domain inversion was also investigated and the results are shown in Figure 1. Both 50× and 20× objective lenses were used for this purpose, and it was found the tighter focusing is not beneficial for poling deep into the crystal. This can be well explained by considering the spherical distortion of an optical system, where more tightly focused beam suffers more serious beam quality deterioration than the loosely focused one.
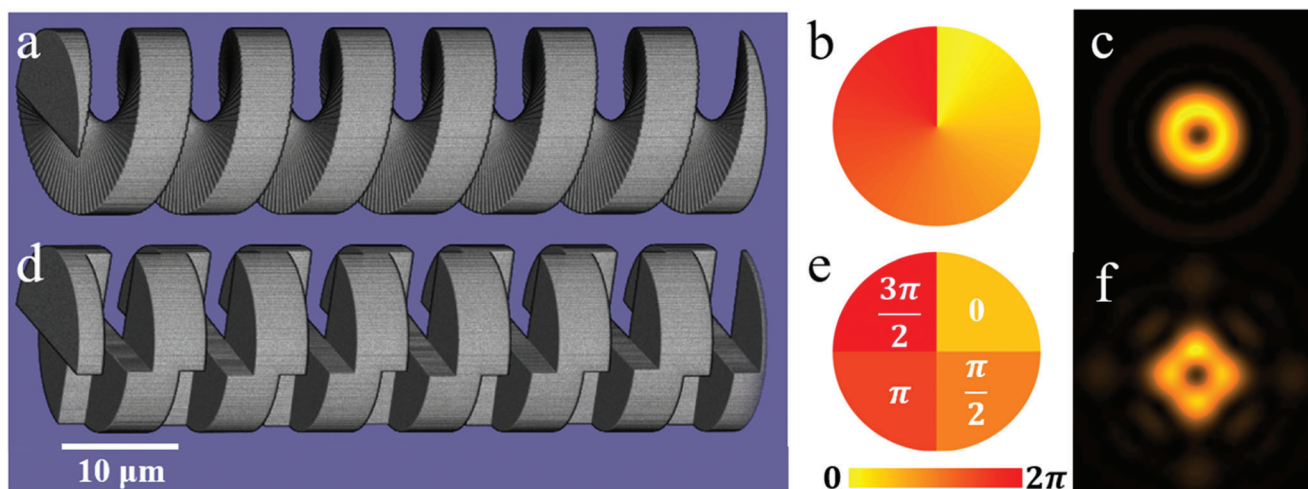
2.2. Reducing the Unwanted Refractive Index Change in the Ferroelectric Laser Poling Process

Intense illuminations of the femtosecond laser pulses not only lead to ferroelectric domain inversion, but also induce modification of the refractive index of the crystal. These small modifications cause unwanted scattering and reflections of optical waves that limit the efficient interaction length inside the nonlinear photonic crystals. A straightforward way to suppress the undesired light-induced refractive index change is substituting the commonly used tightly focused writing beam with a loosely focused one. **Figure 2**a,b show the optical microscope images of nonlinear domain gratings written at the same conditions, but with 50× and 20× objective lenses, respectively. It is clearly seen that the refractive index changes induced by 20× objective lens are much weaker. To further characterize the refractive index change, the linear optical diffraction experiment was conducted,

and the results are shown in Figure 2c,d, respectively. The first three orders of linear diffractions were observed from the sample fabricated with 50× objective, while no diffraction was observed from the 20× objective fabricated sample. We also estimated the light-induced refractive index change by comparing the intensity ratio between different diffraction orders from the sample written with 50× objective lens.[11,24] The obtained value of $\approx 3.5 \times 10^{-5}$ is comparable with that in the electric field poled sample $\approx 1.5 \times 10^{-5}$ (measured using the same method), and much smaller than those produced by the nonlinearity erasure method.[11] Furthermore, we measured the scattering loss of a 200 µm long NPC fabricated by 50× objective lens, and 4% linear loss was measured. For exactly the same NPC structure fabricated by 20× objective lens, the linear loss is negligible.

2.3. An Example of Efficient Nonlinear Interactions in 3D Nonlinear Photonic Crystals

We concentrate on improving the efficiency of nonlinear volume holography in 3D NPCs, taking the second harmonic vortex beam generation (topological charge $l_c = 1$) from a fundamental Gaussian beam as an example. The geometry of collinear interaction, namely the fundamental (FW) and the second harmonic (SH) beams propagating along the same direction inside the nonlinear crystal, is utilized to eliminate the spatial walk-off effect and hence maximizing the efficient interaction volume. The calculated and binarized nonlinear holographic structure is shown in **Figure 3**a, assuming a fundamental wavelength of 1200 nm. This is a spiral structure with the duty cycle 50% for the best conversion efficiency (see Methods for more details). While the structural binarization may cause appearance of higher-order diffraction in Fourier space, its influence on the second harmonic generation is negligible as those high-order components do not fulfill the phase matching condition and give rise to very weak signals. The far-field wavefront (phase) and intensity profile of the second harmonic simulated using the fast Fourier transform method are shown in Figure 3b,c, respectively.[15] The phase singularity and the corresponding dark center of the second harmonic donut beam are clearly seen. Besides optimizing the nonlinear volume holographic structure design, the natural properties of the nonlinear medium should also be utilized to achieve high conversion efficiency. The propagation direction and polarization of interacting beams should be selected to allow the usage of the maximal nonlinear coefficient of the nonlinear crystal.

**ADVANCED
SCIENCE NEWS**

www.advancedsciencenews.com

**ADVANCED
OPTICAL
MATERIALS**

www.advopticalmat.de

Figure 3. 3D nonlinear holograms (3D NPC) for SH vortex generation. a) The ideal spiral $\chi^{(2)}$ structure and the calculated b) transverse phase and c) intensity distribution of the generated second harmonic beam in far-field. d) The discretization of four segment structure and the calculated e) phase and f) intensity of the corresponding second harmonic.
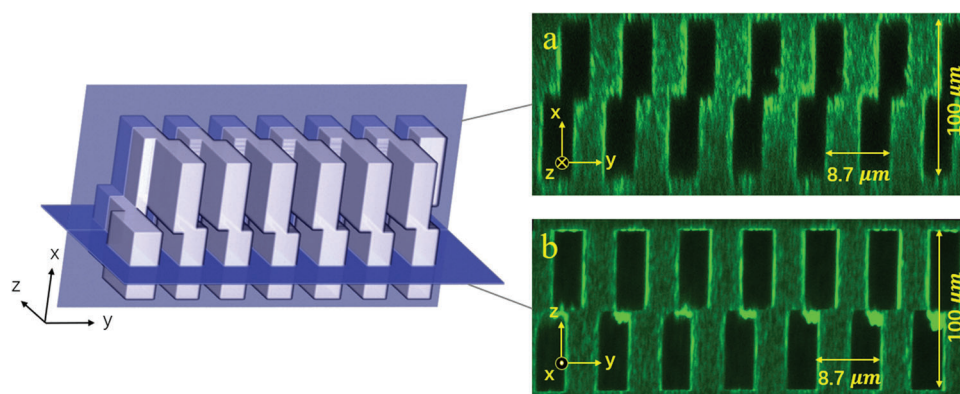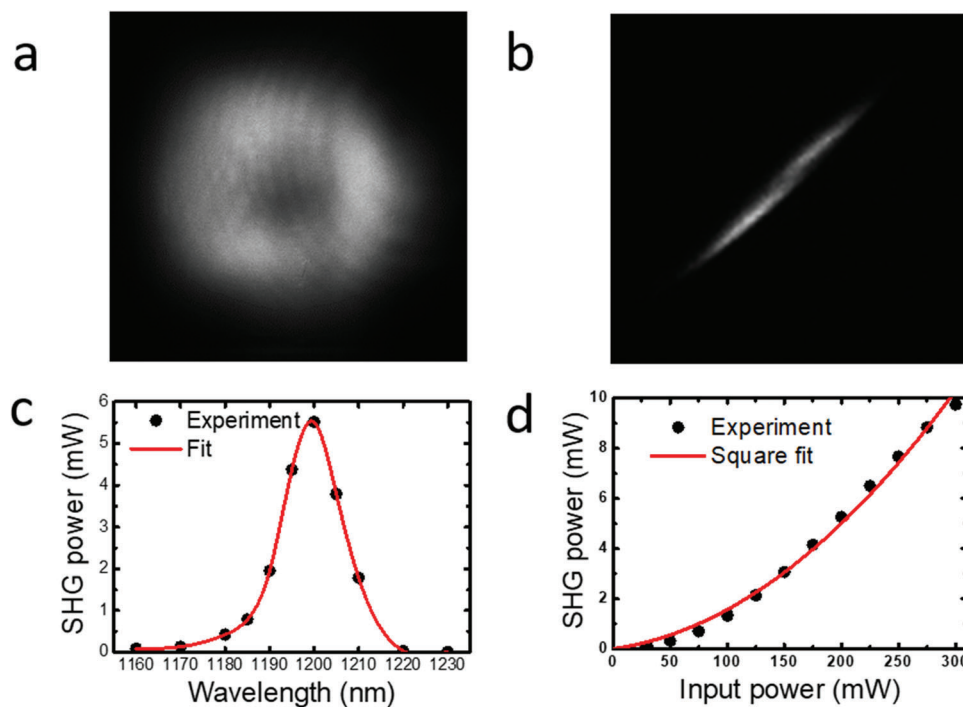

Figure 4. The experimentally fabricated 3D nonlinear holographic structure. a,b) The cross section images of the structures in the *xy* and *yz* planes, imaged by using the Čerenkov second harmonic microscopy.[23] The images in the right column are enlengthen about 5 times in *y*-direction for better visualization. The plot on the left column illustrates the orientations of the imaging planes in the whole sample. The rectangles represent the poled domain regions. The crystal is originally unpoled.

The spiral structure shown in Figure 3a exhibits continuously varying spatial profile, the fabrication of which is challenging as the optical poling has relatively low resolution along the depth direction. Moreover, the commonly used motorized stages in the laser writing platform could easily introduce errors when such kind of smooth structures are fabricated, which may eventually ruin the phase matching function of the NPC.[16] The discretized version of the continuous structure consisting of multiple slabs is more desirable for the laser writing platform. Hence the smooth spiral domain pattern was discretized to form a four-segment structure, as shown in Figure 3d. The design principle is to use four inverted domain segments to generate second harmonic whose phase is shifted by 0, 90°, 180°, and 270° in each segment, respectively. In this way, the phase singularity of the spiral structure is imitated. Practically, the desired shift of 90 degrees between neighboring segments is realized by longitudinally shifting nonlinearity grating of each segment by the distance of $\Lambda/4$, where Λ is the QPM periodicity at the designed wavelength.[21]

The calculated wavefront phase and intensity of the second harmonic generated in this discretized structure are plotted in Figure 3e,f, respectively. It can indeed be seen, that the donut beam is obtained despite of the discretization of four segment structure. In fact, in linear optics, analogous multi-fold transmissive and reflective structure was used in the past to generate optical vortices from incoming laser beam.[25–26] Notice that by increasing the number of segments from four to six and eight, the beam quality of the second harmonic donut can be obviously improved, but the four segments are the easiest to fabricate. Therefore, we use the four segments in the following experiment.

Using the femtosecond laser poling technique, the designed 3D nonlinear holographic structure was fabricated in the CBN crystal (see Methods for details). The Čerenkov second harmonic microscopy was used to visualize the fabricated domain structure, with two cross-section images (*xy* and *yz* planes) being shown in **Figure 4**a,b, respectively. This structure was designed for the second harmonic vortex beam generation at

**ADVANCED
SCIENCE NEWS**

www.advancedsciencenews.com

**ADVANCED
OPTICAL
MATERIALS**

www.advopticalmat.de

Figure 5. The second harmonic vortex beam generation with a pulsed fundamental Gaussian beam. a) The emitted vortex beam directly recorded by the CCD camera after passing through a short pass filter to eliminate the fundamental. b) Astigmatic transformation of the generated vortex beam by a cylindrical lens. A single dark stripe in the middle of the pattern confirms, $l_c = 1$, topological charge of the vortex beam. c) The Wavelength dependence of the power of the SH vortex beam, showing the resonance at 1200 nm. d) Output power versus input power dependence recorded for the resonance peak visible in (c), i.e., when the fundamental wavelength is set to 1200 nm.
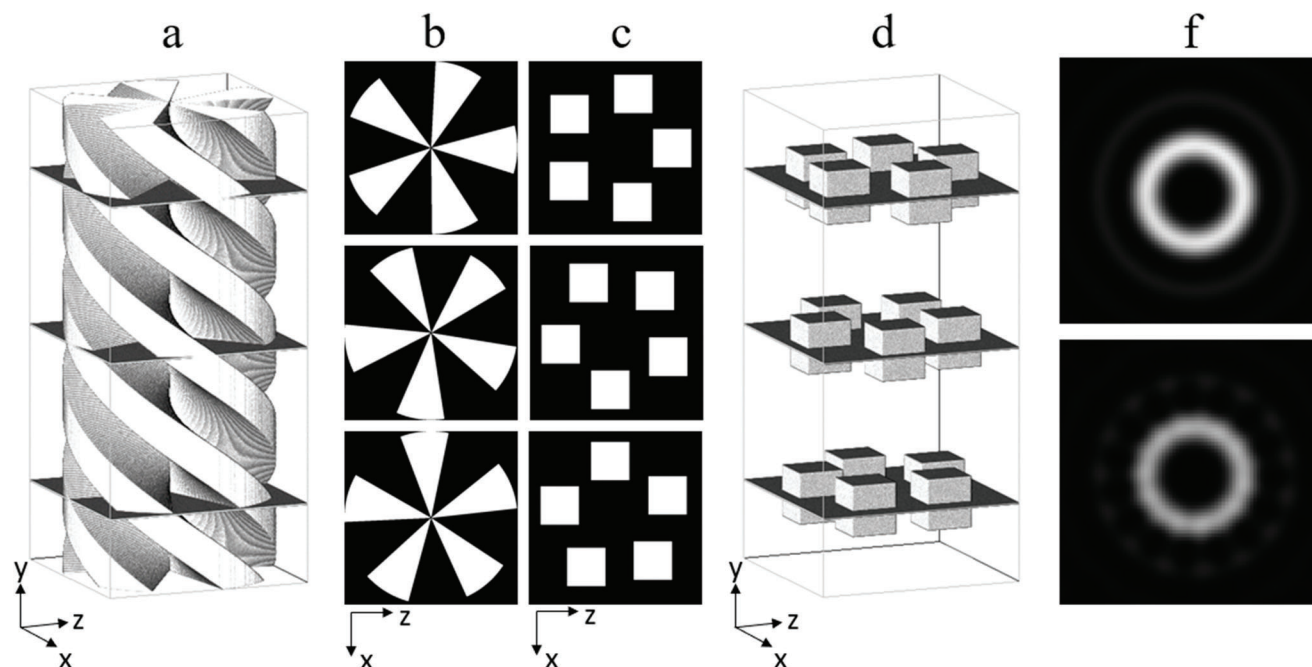
a fundamental wavelength of 1200 nm. The periodicity along y direction is 8.7 µm, which is determined by nonlinear volume holography theory (see Experimental Section) and the cross-sectional dimensions and the length of each poled segment are 50×50 µm^2 and 1 mm, respectively.

The second harmonic generation experiment was performed with a pulsed optical parametric oscillator system which deliveries 200 fs pulses with tunable spectral range from 800 to 1600 nm. Input fundamental beam propagates along the y-axis of the crystal with the polarization along z-axis, such that the maximal nonlinear coefficient d_{33} can be used (see Experimental Section for more details). **Figure 5**a shows the generated SH vortex beam recorded by a CCD camera, which clearly shows the dim center of the donut-shape beam. The topological charge of the beam was checked by transmitting it through a cylindrical lens. Single dark stripe visible in the focus corresponds to the designed topological charge $l_c = 1$ (Figure 5b).

The SHG power dependency on the fundamental wavelength is depicted in Figure 5c, with the highest SHG power peaks at 1200 µm FW wavelength as designed. All data points are collected with 200 mW power of the incident fundamental beam. The FWHM of the SH power peak is ≈20 nm width because of broadband property of pulsed laser as well as the finite size of 3D NPC. Higher order peaks are not shown in this plot as the large phase mismatch makes the higher order peaks fall out of the OPO tunning range. Figure 5d shows both experimental measured data and theoretical quadratic fit of SH power as a function of input FW power. The optimal FW wavelength 1200 nm was

used to obtain this set of data. The experimental and theoretical results match perfectly , which confirms the second order nonlinear process. The SH power reached 9.9 mW with 300 mW pumping power and 4.6% conversion efficiency was achieved when excluding the reflection losses on both crystal surfaces. The normalized conversion efficiency is 2.9×10^{-6} W^{-1}, which is at least four orders of magnitude more compared to previous reported results from 3D wave shaping NPC.[15,20] Such big improvement of efficiency could significantly broaden the applications of 3D NPC.

Additionally, a CW laser was also used as a pumping source to generate the SH vortex beam. Another 3D NPC was designed and fabricated under same methods as stated in previous sections, but with a periodicity matched with the CW laser wavelength of 1560 nm. The volume of this 3D NPC is $100 \times 100 \times 1000$ µm^3, with a periodicity of 17.51 µm and it carries topological charge $l_c = 1$. Using the same SHG method applied on the pulsed laser, an SH vortex beam was generated under the CW laser pumping. The second harmonic power reached 6 µW with a 710 mW pumping power, corresponding to a normalized efficiency ≈1.2×10^{-5} W^{-1}. The measured CW-pumped efficiency is higher than that of the pulsed case, which is reasonable as the CW scheme is free of group velocity dispersion. CW laser beams have excellent monochromatic property and hence suitable to achieve stronger quasi-phase matched interaction. Hence the realization of efficient CW second harmonic generation in 3D NPC paves the way to achieving highly dense frequency-division multiplexing and multiphoton quantum states.

**ADVANCED
SCIENCE NEWS**

www.advancedsciencenews.com

**ADVANCED
OPTICAL
MATERIALS**

www.advopticalmat.de

Figure 6. The generalized structure sampling method to facilitate more complex 3D NPCs. a) The ideal fivefold helical structure for collinear generation of the second harmonic vortex beam (along *y* axis) with topological charge $l_c = 5$. b) The cross section structures obtained by sampling at three discrete planes. c,d) The simplified 2D and 3D structures by replacing the five segments containing complex and continuing varied spatial details with rectangular and cuboids, respectively. e,f) The simulated far field intensity distributions of the second harmonic beams from the ideal fivefold helical structure and the simplified structure, respectively.

2.4. A Generalized Sampling Method to Facilitate More Complex 3D NPCs

The experiments described above dealt with the relatively simple 3D spiral structure, which can be discretized into four segments for efficient collinear generation of second harmonic vortex beam. But real cases can be more complex. For example, the cross-sectional structures of 3D NPCs may be too complicated to directly fabricate with the laser poling technique. Furthermore, structure samplings may become more challenging if the QPM periodicity goes beyond the resolution ability of the laser poling technique. Therefore, there is a need to establish a general design method to facilitate fabrications of more complex 3D NPCs.

Here we consider a multi-helical structure for the generation of collinear second harmonic vortex with high topological charge ($l_c = 5$).[21] The fundamental wavelength is selected to be 800 nm. This corresponds to a longitudinal periodicity of 1.8 μm, which already approaches the resolution ability of the current laser poling technique. Plots in **Figure 6** illustrate the procedures of the proposed design method. First, the ideal five-fold helical structure is established using the nonlinear volume holography theory. In fact, this is a complex structure consisting of five mutually entangled spirals (Figure 6a), which is hard to fabricate. For simplification, in the next step one must select a sampling period, which can be even larger than the QPM period. For example, here we take a sampling period of 3 μm and conduct the sampling along the *y*-axis to acquire a series of cross sections. In Figure 6b, three examples of such sampled cross-sections are shown. Step 3, using the digital image processing algorithm, it is easy to find the centroid of each segment in the cross-section pattern and replace

all the segments with cuboids to obtain a fabrication friendly 3D NPCs, as shown in Figure 6c,d. The dimensions of such cuboids determine the duty cycles of the whole structure. It is worth noting that the sampling period should not be multiples of the QPM period. Otherwise, the sampling becomes invalid because all the cross section pattens will be the same.

The simulated intensity distributions of the SH beams from the ideal five-fold helical structure and the simplified structure are shown in Figure 6f, respectively. Clearly the high topological charge vortex beam could be generated from both structures. The conversion efficiency of the simplified structure is nearly 20 times lower than that of the ideal one, but this side effect could be easily compensated by fivefold increase of the length of the structure.

3. Conclusion

We have employed femtosecond laser poling technique to fabricate 3D nonlinear photonic crystals and improved the nonlinear interaction efficiency by more than four orders of magnitude. In the experiment, we have overcome the major challenges that had hindered the fabrication of large-scale 3D nonlinear photonic crystals. By properly selecting the polarization of the writing laser beam with respective to the crystallographic orientation, we have avoided the birefringence-induced multi-focusing on optical beam such that the ferroelectric domains can be written as deep as 2628 μm inside the second-order nonlinear crystal. Meanwhile, the undesired light-induced refractive index changes have been suppressed by optimizing the focusing condition of the writing laser beam, which is critical to achieve a long efficient

**ADVANCED
SCIENCE NEWS**

www.advancedsciencenews.com

**ADVANCED
OPTICAL
MATERIALS**

www.advopticalmat.de

interaction length in the nonlinear photonic crystal. As a real example, the collinear generation of second harmonic vortex beam from a fundamental Gaussian beam was experimentally realized in a 1 mm long 3D nonlinear photonic crystal. The measured conversion efficiencies were 2.9×10^{-6} W^{-1} from a femtosecond laser pump and 1.2×10^{-5} W^{-1} from a CW laser pump, respectively. It is interesting to mention that the same structure we studied here can be used for detection of specific near-infrared OAM beams at visible wavelengths. For example, a fundamental beam with topological charge of -1 will be converted to a Gaussian-like mode at the second harmonic, that can be easily detected by having a pinhole in front of the detector.[27] We note that the methods we used here can be easily implemented for generating other types of beams, such as Hermite-Gaussian beams, Bessel beams, and Airy beams. The experimental realization of such efficient nonlinear interactions in 3D nonlinear photonic crystals, especially the scheme of CW pump, laid the foundations for fully utilizing the advantages of 3D NPCs in nonlinear photonics and quantum applications such as the nonlinear orbital angular momentum multiplexing and the realization of high-dimensional entangled source.

4. Experimental Section

Design of the Nonlinear Volume Hologram: The nonlinear holographic structures are obtained using the computer-generated interference fringes between the nonlinear polarization wave ($\propto E_{FF}^2$) and the second harmonic (E_{SH}) with predesigned wave fronts.[14] The fundamental beam is assumed to be a plane wave, which can be approximately replaced by a loosely focused Gaussian beam in experiment. For the generation of second harmonic vortex with topological charge l_{c}, the amplitude of the fundamental and the second harmonic waves can be written as $E_{FF} = Ae^{i(k_1 y - \omega t)}$ and $E_{SH} = Be^{i(k_2 y - 2\omega t + p(x,z))}$, where k_1 and k_2 are the corresponding wave vectors of fundamental and second harmonic beam and $p(x, z) = \tan^{-1} z/x$ is the vortex phase profile. Since the ferroelectric domain reversal could only change the sign of the second nonlinearity, a binary structure is required:

$$f(x, y, z) \propto \text{sign} [\cosh (2k_1 y - 2k_2 y - p(x, z))] \qquad (1)$$

where $|k_1| = 2\pi n_{1e}/\lambda$ and $|k_2| = 2\pi n_{2e}/\lambda$ are wavevectors of the fundamental and second harmonic waves, and n_{1e} and n_{2e} are the corresponding refractive indices, respectively. These values were taken using the refractive index of the CBN crystal reported.[28]

Optical Poling of the CBN Crystal: A custom-built laser writing system was used for the optical poling.[10] The writing laser beam was generated from a femtosecond oscillator (MIRA, Coherent) operating at 780 nm with a pulse duration of 180 fs and a repetition rate of 76 MHz. The power and polarization of the writing laser beam could be continuously varied by using a half wave plate followed by a polarizer, before focusing it into the CBN crystal by an objective lens. For comparisons two objective lenses were used. One is with magnification 20× and numerical aperture NA = 0.4, and the other is 50× and NA = 0.65. The CBN crystal was mounted on a translational stage that could be positioned along three orthogonal directions automatically.

To fabricate the nonlinear photonic structure of four segments, the writing laser beam was incident from the x-surface and scanned along z-direction for 50 µm with a velocity of 0.02 mm s⁻¹. In this way, an inverted domain stack with dimensions ≈20 µm (x) × 3 µm (y) × 50 µm (z) was obtained. Afterwards the writing beam was blocked by an automatic shutter and the sample was translated back to the original position, then it moved a small distance along y-direction and the process was repeated to produce another inverted domain stack of the same dimensions. The dis-

tance between these neighboring stacks was set to be 1 µm to ensure that they merged to form a large-scale domain block. By repeating the above process N times, inverted domains in dimensions ≈20 µm (x) × N µm (y) × 50 µm (z) were created. To further enlarge the scale of inverted domain block at x-direction, the sample was transferred along x-direction for 20 µm and the domain inversion steps above were repeated to increase the domain length at x-direction. This large-scale single domain block forms the basic unit of the four-segment structure. The nonlinear grating was fabricated by producing such blocks periodically along y-axis. The period was 8.7 µm to for QPM at 1200 nm and the width of each block (along y direction) was 4 µm to approach the optimal duty cycle of 50% and hence maximize the conversion efficiency. The four-segments $\chi^{(2)}$ structure was constructed by fabricating four nolinearity gratings and shifting them along the y-direction by 2.175, 4.350, and 6.525 µm, respectively (see Figure 4).

The four-segments domain structure was fabricated at a depth range of 500 to 600 µm below the x-surface of the crystal. The laser poling power was kept as 450 mW. This value was just 20 mW higher than the laser poling threshold to minimalize the undesirable refractive index changes. The fabrication time is roughly proportional to the volume of the nonlinear photonics crystal, for a 100 µm ×100 µm ×1000 µm sample the fabrication time is ≈8 h.

Experimental Schemes for Second Harmonic Vortex Beam Generation: In the scheme of pulsed pumping, the fundamental beam was originated from the Coherent Chameleon OPO system. The pulse duration is 200 fs, repetition rate is 80 MHz, and the wavelength is tunable between 800 and 1600 nm. The beam was loosely focused into the nonlinear photonic structure by a lens (focal length of 45 mm) and the Rayleigh length was estimated ≈10 mm to ensure the plane wave approximation. The beam size was ≈90 µm. The fundamental beam propagated along the y-axis of the sample and linearly polarized along z-axis to generate the second harmonic via the largest nonlinear coefficient d_{33}. A short-pass filter was placed behind the sample to block the fundamental beam while the outgoing spatially shaped second harmonic was directly recorded by a CCD. The power of SH was measured by a power meter.

For SHG in CW regime, the fiber output of a CW tunable laser (TSL-570) was injected to an erbium-doped optical fiber amplifier (EDFA). Then the amplified CW laser was focused by a lens with a focal length of 35 mm to the femtosecond laser written grating. The position of the grating sample can be adjusted to meet the best coupling. A long-pass dichroic mirror was used to reflect the SHG light into the power meter.

Theoretical Conversion Efficiency: The conversion efficiency of long NPC depends on the properties of excitation laser, for short pulsed laser the temporal walk-off phenomenon is not negligible and the efficiency should be calculated by equation:[29]

$$\eta = \frac{16\pi^2 d_{eff}^2 P_\omega l_t t_{rep}}{n_\omega n_{2\omega} c \varepsilon_0 \lambda_1^3 \tau} \frac{L}{b'} \qquad (2)$$

For CW laser the temporal walk-off is negligible and the efficiency could be calculated by equation [29]:

$$\eta = \frac{4\omega^2 d_{eff}^2 L^2 P_\omega t_{rep}}{n_\omega n_{2\omega} c^3 \varepsilon_0 \lambda_1 b' \tau} \qquad (3)$$

and normalized conversion efficiency:

$$\eta_{norm} = \frac{P_{2\omega}}{P_\omega^2} \frac{\tau}{t_{rep}} = \frac{\eta}{P_\omega} \frac{\tau}{t_{rep}} \qquad (4)$$

where d_{eff} is the effective nonlinear coefficient, t_{rep} is the repetition period, L is the length of the NPC, c is the speed of light, ε_0 is the vacuum permittivity, τ is the pulse width, b' is the confocal parameter of the input beam, l_t is the walk-off length, and n_ω and $n_{2\omega}$ are refractive indices of the FW and SH, respectively.

Two 1-mm long 3D NPC demonstrated in this work were tested under fs laser and CW laser respectively. The 50% optimal duty cycle was achieved

ADVANCED
SCIENCE NEWS
www.advancedsciencenews.com

ADVANCED
OPTICAL
MATERIALS
www.advopticalmat.de

on both samples which give an effective nonlinear coefficient as high as $d_{eff} = 2.86 \times 10^{-12}\,\frac{m}{V}$, which is about 13 times higher than previous reported work,[20] and boots the efficiency for 2 orders of magnitude. For the fs laser pump, the theoretical normalized efficiency is $3.3 \times 10^{-6}\,\text{W}^{-1}$ and the measured efficiency is $2.9 \times 10^{-6}\,\text{W}^{-1}$. For the CW laser pump, the theoretical normalized efficiency is $1.6 \times 10^{-5}\,\text{W}^{-1}$ and the measured efficiency is $1.2 \times 10^{-5}\,\text{W}^{-1}$. It is natural that the efficiency measured with pulsed laser is lower as the temporal walk-off phenomenon limits the SHG process. For the CW tested sample, it is already quite close to the theoretical optima and the loss mainly came from the imperfection of the poled domain structures.

Conflict of Interest

The authors declare no conflict of interest.

Data Availability Statement

The data that support the findings of this study are available from the corresponding author upon reasonable request.

[1] J. A. Armstrong, N. Bloembergen, J. Ducuing, P. S. Pershan, *Phys. Rev.* **1962**, *127*, 1918.
[2] V. Berger, *Phys. Rev. Lett.* **1998**, *81*, 4136.
[3] S. N. Zhu, Y. Y. Zhu, N. B. Ming, *Science* **1997**, *278*, 843.
[4] C. Canalias, V. Pasiskevicius, M. Fokine, F. Laurell, *Appl. Phys. Lett.* **2005**, *86*, 181105.
[5] N. V. Bloch, K. Shemer, A. Shapira, R. Shiloh, I. Juwiler, A. Arie, *Phys. Rev. Lett.* **2012**, *108*, 233902.
[6] T. Ellenbogen, N. Voloch-Bloch, A. Ganany-Padowicz, A. Arie, *Nat. Photonics* **2009**, *3*, 395.
[7] G. A. Magel, M. M. Fejer, R. L. Byer, *Appl. Phys. Lett.* **1990**, *56*, 108.
[8] N. G. R. Broderick, G. W. Ross, H. L. Offerhaus, D. J. Richardson, D. C. Hanna, *Phys. Rev. Lett.* **2000**, *84*, 4345.
[9] X. Chen, P. Karpinski, V. Shvedov, K. Koynov, B. X. Wang, J. Trull, C. Cojocaru, W. Krolikowski, Y. Sheng, *Appl. Phys. Lett.* **2015**, *107*, 141102.
[10] T. Xu, K. Switkowski, X. Chen, S. Liu, K. Koynov, H. Yu, H. Zhang, J. Wang, Y. Sheng, W. Krolikowski, *Nat. Photonics* **2018**, *12*, 591.
[11] D. Wei, C. Wang, H. Wang, X. Hu, D. Wei, X. Fang, Y. Zhang, D. Wu, Y. Hu, J. Li, S. Zhu, M. Xiao, *Nat. Photonics* **2018**, *12*, 596.
[12] J. Thomas, V. Hilbert, R. Geiss, T. Pertsch, A. Tünnermann, S. Nolte, *Laser Photon Rev* **2013**, *7*, L17.
[13] S. Keren-Zur, T. Ellenbogen, *Nat. Photonics* **2018**, *12*, 575.
[14] S. Liu, L. M. Mazur, W. Krolikowski, Y. Sheng, *Laser Photonics Rev.* **2020**, *14*, 2000224.
[15] P. Chen, C. Wang, D. Wei, Y. Hu, X. Xu, J. Li, D. Wu, J. Ma, S. Ji, L. Zhang, L. Xu, T. Wang, C. Xu, J. Chu, S. Zhu, M. Xiao, Y. Zhang, *Light Sci Appl* **2021**, *10*, 146.
[16] J. Imbrock, L. Wesemann, S. Kroesen, M. Ayoub, C. Denz, *Optica* **2020**, *7*, 28.
[17] A. Karnieli, S. Tsesses, G. Bartal, A. Arie, *Nat. Commun.* **2021**, *12*, 1092.
[18] E. Rozenberg, A. Karnieli, O. Yesharim, S. Foley-Comer, S. Trajtenberg-Mills, D. Freedman, A. M. Bronstein, A. Arie, *Optica* **2022**, *9*, 602.
[19] C. Xu, S. Huang, Q. Yu, D. Wei, P. Chen, S. Nie, Y. Zhang, M. Xiao, *Phys. Rev. A* **2021**, *104*, 063716.
[20] D. Wei, C. Wang, X. Xu, H. Wang, Y. Hu, P. Chen, J. Li, Y. Zhu, C. Xin, X. Hu, Y. Zhang, D. Wu, J. Chu, S. Zhu, M. Xiao, *Nat. Commun.* **2019**, *10*, 4193.
[21] A. Bahabad, A. Arie, *Opt. Express* **2007**, *15*, 17619.
[22] P. Karpinski, V. Shvedov, W. Krolikowski, C. Hnatovsky, *Opt. Express* **2016**, *24*, 7456.
[23] Y. Sheng, A. Best, H. J. Butt, W. Krolikowski, A. Arie, K. Koynov, *Opt. Express* **2010**, *18*, 16539.
[24] F. Y. Jian-guan Hua, Z.-N. Tian, Y.-H. Yu, Y.-S. Yu, *J. Laser Micro/Nanoeng.* **2017**, *12*, 207.
[25] R. P. C. C. M. W. Beijersbergen, M. Kristensen, J. P. Woerdman, *Opt. Commun.* **1994**, *112*, 321.
[26] G. Campbell, B. Hage, B. Buchler, P. K. Lam, *Appl. Opt.* **2012**, *51*, 873.
[27] K. Shemer, N. Voloch-Bloch, A. Shapira, A. Libster, I. Juwiler, A. Arie, *Opt. Lett.* **2013**, *38*, 5470.
[28] M. Eßer, M. Burianek, P. Held, J. Stade, S. Bulut, C. Wickleder, M. Mühlberg, *Cryst. Res. Technol.* **2003**, *38*, 457.
[29] A. M. Weiner, *Ultrafast optics*, Wiley, Hoboken, N.J **2009**.